Laser and Particle Beams (2012), *30*, 87–93.

doi:10.1017/S0263034611000711

Large field-of-view X-ray imaging by using a Fresnel zone plate

XIAO-FANG WANG, JIN-YU WANG, XIAO-HU CHEN, XIN-GONG CHEN, AND LAI WEI
Department of Modern Physics, University of Science and Technology of China, Hefei, China

(RECEIVED 2 February 2011; ACCEPTED 26 July 2011)

Abstract

To diagnose the implosion of a laser-driven-fusion target such as the symmetry, the hydrodynamic instability at the interface, a high-resolution, large field-of-view kilo-electron-volt X-ray imaging is required. A Kirkpatrick-Baez (K-B) microscope is commonly used, but its field of view is limited to a few hundred microns as the resolution decreases rapidly with the increase of the field of view. A higher resolution could be realized by using a Fresnel zone plate (FZP) for imaging. Presented in this work is a numerical study on the imaging properties of an FZP at Ti-*K*α wavelength of 0.275 nm, and a comparison to a K-B imager. It is found that the FZP can realize not only a resolution better than 1 μm, but also a field-of-view larger than 20 mm when the FZP is illuminated by X-rays of spectral bandwidth less than 1.75%. These results indicate the feasibility of applying the FZP in high-resolution, large field-of-view X-ray imaging.

Keywords: Fresnel zone plate; High resolution; Large field-of-view; Laser fusion target; X-ray imaging

INTRODUCTION

In laser-driven inertial confinement fusion, a symmetric, highly convergent implosion of a target is necessary (Lindl *et al.*, 2004). This requires not only the irradiation uniformity of laser beams or X-rays, but also the suppression of hydrodynamic instabilities. For example, the Rayleigh-Taylor instability will cause the mixing of pusher and fuel at the interface in a target, or even the target shell breakup. In experiments, to diagnose the symmetry of implosion, the hydrodynamic instability and its growth, or the area density of an imploded target, backlighting radiography is usually adopted, i.e., a kilo-electron-volt X-ray beam emitted from a backlighter goes through the target and is received by an imager to the target.

Several imagers such as pinholes, Kirkpatrick-Baez (K-B) microscopes, and curved crystals have been used for X-ray imaging (Koch *et al.*, 2003; Marshall *et al.*, 1998; Gotchev *et al.*, 2003). Pinhole imaging is the simplest, but it is limited by low collection angle and the spatial resolution by the pinhole size, on the order of 5–10 μm. The other two have larger collection angle and the theoretical resolution is better. K-B microscopes have been widely used, for example, in experiments of equation-of-state measurements, hydrodynamic instability investigations (Collins *et al.*, 1998; Gotchev *et al.*, 2003). Nevertheless, affected by aberrations or the surface quality of the K-B mirrors, the field of view (FOV) was limited to a few hundred microns and the best resolution 2–3 μm (Marshall *et al.*, 1999; Mu *et al.*, 2009). For some issues, such as the plasma density gradient at interfaces (Azechi *et al.*, 2007), or the filamentation of electron beams in dense plasmas (Taguchi *et al.*, 2001), a higher resolution is necessary for X-ray imaging diagnostics. Taking into account of FOV for imaging a laser-fusion target, an ideal imager should have an FOV on the order of 1 mm, and a spatial resolution as good as 1 μm.

Fresnel zone plate (FZP) imaging, based on the diffraction of X-rays, has provided in X-ray microscopy the highest spatial resolution, as high as 10 nm (Chao *et al.*, 2005; Tian *et al.*, 2008). There appeared experiments of using FZP's in high-resolution X-ray imaging of laser plasmas (DaSilva *et al.*, 1992; Cauchon *et al.*, 1998; Azechi *et al.*, 2003). Different from X-ray microscopy in which the FOV is on the order of 10 μm, for imaging a laser-fusion target, the FOV has to be on the order of 1 mm. On the other hand, 1-μm spatial resolution should be enough for imaging a laser-fusion target. So it is necessary to reconsider the FZP imaging related to fusion diagnostics. As FZP imaging works at normal-incidence illumination, aberrations are avoided. It is anticipated that the FOV of FZP imaging should be larger than that of a K-B microscope, and the spatial resolution better as well.

Address correspondence and reprint requests to: Xiao-Fang Wang, Department of Modern Physics, University of Science and Technology of China, Hefei, Anhui 230026, China. E-mail: wang1@ustc.edu.cn

In this work, the spatial resolution and the FOV of FZP imaging at the Ti-*K*α line (0.275 nm) are analyzed and compared to the imaging of a K-B microscope. The work is organized as follows. First, the FOV of the K-B microscope is presented. Next the analyses of FZP imaging are presented, including the imaging principle, the numerical study on the FOV, and the influence of polychromatic light. Finally, the properties of the two imagers are compared and conclusions are given.

IMAGING OF A K-B MICROSCOPE

For a single spherical mirror, e.g., the left one in Figure 1, the imaging for paraxial rays in the meridian plane (*y*-*z* plane in Fig. 1) and the sagittal one (*x*-*z* plane) separately satisfies (Kirkpatrick & Baez, 1948):

$$\frac{1}{u}+\frac{1}{\mathrm{v}}=\frac{2}{R\sin\theta}, \tag{1}$$

$$\frac{1}{u}+\frac{1}{\mathrm{v}'}=\frac{2\sin\theta}{R}. \tag{2}$$

In which u, v, or v′ are the distances from the source to the mirror, and the mirror to the image, respectively, R is the radius of the mirror, and θ is the grazing incidence angle. Since θ is small, severe astigmatism exists so that the image in the meridian plane does not overlap with that in the sagittal plane. When the second same spherical mirror is combined orthogonally with the first one, which is called a K-B microscope (Kirkpatrick & Baez, 1948), and by choosing the two grazing-incidence angles θ_1 and θ_2, the images of the meridian and the sagittal planes could overlap, and a two-dimensional stigmatic image could be formed on the image plane. For this case:

$$\frac{1}{u}+\frac{1}{\mathrm{v}+w}=\frac{2}{R\sin\theta_1}, \tag{3}$$

$$\frac{1}{u+w}+\frac{1}{\mathrm{v}}=\frac{2}{R\sin\theta_2}. \tag{4}$$

In which w is the spacing of the two mirrors. Although a stigmatic image is formed, primary aberrations like the spherical aberration still exist (Kirkpatrick & Baez, 1948). Ray-tracing simulations are usually used to analyze the imaging of a K-B microscope.

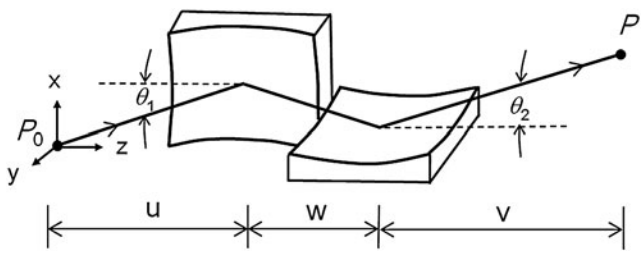

Fig. 1. The schematic diagram of K-B microscope imaging.

A home-made code was developed for the ray-tracing simulation (Wang *et al.*, 2010). Briefly, the numerical recipe of the code is based on the coordinate transformation when tracing each ray of light. The point spread function is calculated for a point source, which is set to locate at different positions on the object plane, to determine the spatial resolution. The spatial resolution is defined as the object-plane size, for its corresponding size as the diameter on the image plane, the circular area contains 68% energy of the image.

Table 1 gives the parameters of the K-B microscope and the simulated setup conditions. The K-B microscope is composed of two gold spherical mirrors. The two grazing-incidence angles θ_1 and θ_2 are selected according to Eqs. (3) and (4). The angles are smaller than the critical angle for total reflection on a gold mirror surface, which is 1.018° at the Ti *K*α line. So an efficient reflection from the mirror surfaces is expected. The image-to-source magnification is $M = 10$, which is typical in experiments. The collecting angle of the K-B microscope is $\Delta\Omega = 4\times10^{-7}$ sr.

Figure 2 presents the simulated spatial resolution of the K-B microscope along two orthogonal directions of the object plane. It shows that at the FOV center, the best resolution is 0.71 μm. Away from the FOV center, the spatial resolution of the K-B microscope decreases rapidly. The FOV for spatial resolutions better than 6 μm is about 400 μm (±200 μm from the FOV center). These results agree with experimental measurements (Marshall *et al.*, 1999; Mu *et al.*, 2009). Aberrations are the main cause. With the increase of the FOV, the aberrations increase, which decrease the spatial resolution and in turn limit the high-resolution or the effective FOV of the K-B microscope.

IMAGING OF AN FZP

Principle of Imaging

Figure 3 shows the schematic of an FZP imaging. Suppose a point source at $P_0(x_0,y_0,z_o)$ on the object plane, its monochromatic radiation amplitude is $A_\lambda(P_0)$. When the light goes through the FZP, whose transmission function is t, the amplitude at point $P(x,y,z)$ on the image plane is given by the Fresnel-Kirchhoff diffraction formula (Born & Wolf, 2001):

$$U(P)=-\frac{iA_\lambda(P_0)}{\lambda}\iint_\Sigma \frac{\tilde{t}(Q)\cdot e^{ik(r+s)}}{rs}\times\left[\frac{\cos(\hat{n},\hat{r})+\cos(\hat{n},\hat{s})}{2}\right]d\Sigma. \tag{5}$$

Table 1. *Parameters of the K-B microscope imaging*

R (m)	w (mm)	θ_1 (degrees)	θ_2 (degrees)	u (mm)	M	$\Delta\Omega$ (sr)
20	7	0.800	0.833	154	10	4×10^{-7}

https://doi.org/10.1017/S0263034611000711 Published online by Cambridge University Press

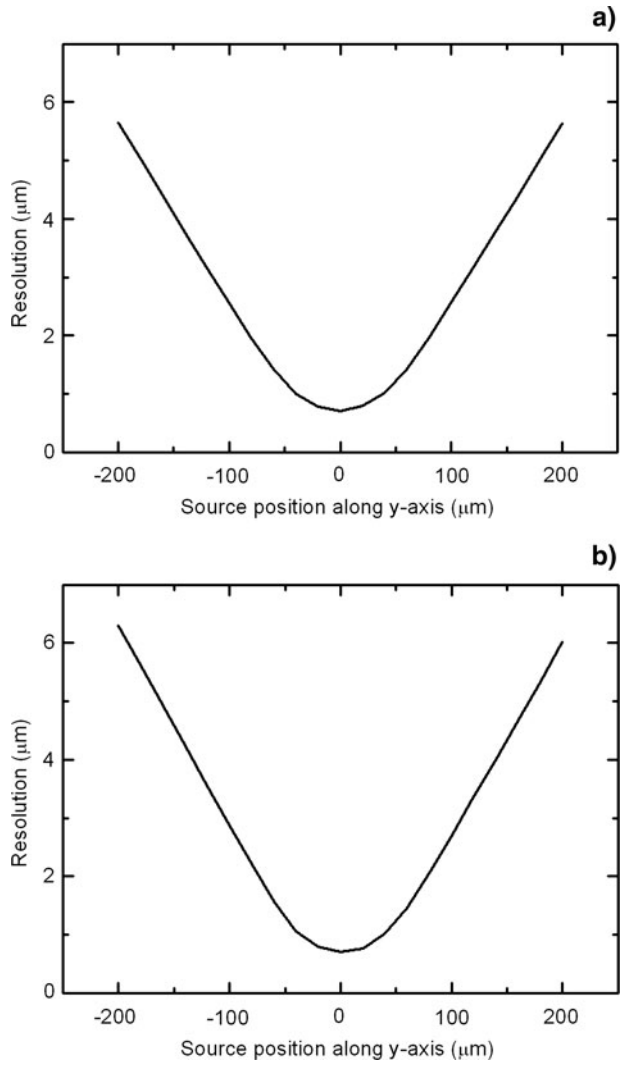

Fig. 2. The spatial resolution of the K-B microscope versus the point source position on the object plane. Position 0 is the FOV center. (**a**) Along x-axis. (**b**) Along y-axis.

In which the integrating area Σ is the FZP. r and s are the distances from P_0 to point $Q(\zeta,\eta,0)$ on the FZP surface, and from Q to P, respectively. $(\widehat{n},\widehat{r})$, $(\widehat{n},\widehat{s})$ are the angles between the FZP normal and the wave vectors of the incident light and the diffracted light, respectively. For applications, there is a good approximation $(\widehat{n},\widehat{r}) \approx 0$, $(\widehat{n},\widehat{s}) \approx 0$. Thus,

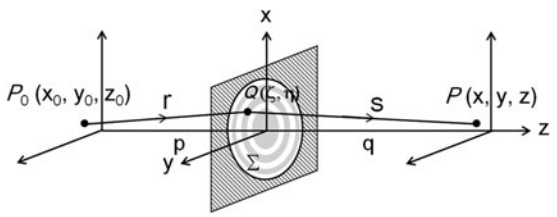

Fig. 3. The schematic diagram of FZP imaging. The optical axis (z-axis) goes through the FZP center and is parallel to the FZP normal.

$\cos(\widehat{n},\widehat{r}) + \cos(\widehat{n},\widehat{s}) = 2$, and Eq. (5) is simplified to:

$$U(P) = -\frac{iA_\lambda(P_0)}{\lambda}\iint_\Sigma \frac{\tilde{t}(Q)\cdot e^{ik(r+s)}}{rs}\,d\Sigma. \tag{6}$$

The intensity is $|U(P)|^2$. It should be pointed out that in Eq. (6), the Fresnel approximation is not used, which was adopted in analyzing an FZP imaging in microscopy. By using the Eq. (6), the FZP imaging of an off-axis source could be analyzed in the regime where the Fresnel approximation cannot be applied (Wang & Wang, 2011).

When including the spectral bandwidth of an incoherent source, the intensity at P is the incoherent superposition:

$$I(P) = \int_\lambda |U(P)|^2 d\lambda. \tag{7}$$

For the FZP, the outer radius of each half-wave zone is related to the primary focus, the first-order diffraction focus, of the FZP, as given by:

$$r_l = \sqrt{l\lambda f}, \quad l = 1, 2, \ldots, N, \tag{8}$$

in which l denotes the lth zone, N is the total number of zones, $f = r_1^2/\lambda$ is the primary focal length, λ is the X-ray wavelength. In the present work, the odd-number zones are set as transparent; the even-number zones are made of the FZP material and are partially transparent to X-rays. So the transmission function $\tilde{t}$ is:

$$\tilde{t} = \begin{cases} 1(\text{odd-number}) \\ e^{-kd(\beta+\delta i)}(\text{even-number}) \end{cases}, \tag{9}$$

in which d is the thickness of the FZP, $k = 2\pi/\lambda$. β and δ are from Henke *et al.* (1993), related to complex refractive index $\tilde{n}$ as: $\tilde{n} = 1 - \delta + i\beta$.

In Figure 3, p and q are the on-axis distances from the FZP to the object plane and the image plane, respectively. p, q, and f satisfy:

$$\frac{1}{p} + \frac{1}{q} = \frac{1}{f}. \tag{10}$$

Eqs. (6)–(10) are the fundamentals for the following numerical studies of the FZP imaging.

The parameters of the FZP are listed in Table 2. The FZP material is gold, thickness $d = 900$ nm, which is optimized for the efficiency of the first-order diffraction (Kirz, 1974). The FZP diameter is $D = 140$ μm, containing a total number of half-wave zones $N = 100$. For the Ti $K\alpha$ line at

Table 2. *Parameters of the FZP imaging*

D (μm)	d (nm)	Δr_{out} (μm)	N	p (mm)	M	ΔΩ (sr)
140	900	0.35	100	196	10	4×10^{-7}

https://doi.org/10.1017/S0263034611000711 Published online by Cambridge University Press

0.275 nm, the primary focal length is 178 mm. For the FZP, the width of the outmost zone is chosen to be 0.35 μm. Albeit the narrower the outmost zone and the more the total number of the zones, the higher the spatial resolution and the larger the collection angle, fabricating such an FZP by X-ray lithography would also become more difficult (Liu *et al.*, 2008). As will be seen in the following, the FZP satisfies the diagnostic requirements.

Spatial Resolution Limit

The spatial resolution limit is usually defined by the Rayleigh criterion. For this, a numerical calculation was done to consider a parallel X-ray beam incident normally onto the FZP. Figure 4 shows the intensity distribution of the primary focus at $q = f$. It is seen that the parallel X-ray beam is focused by the FZP to a tiny spot. The width from the intensity peak to the first minimum is 0.43 μm, corresponding to an angular width $\Delta\theta_m = 2.4 \times 10^{-6}$ rad. Therefore, according to the Rayleigh criterion, the angular resolution limit is 2.4×10^{-6} rad, and the spatial resolution limit is $\Delta r_m = f \cdot \Delta\theta_m = 0.43$ μm.

An analytical theory (Stigliani *et al.*, 1967) shows that when $N > 200$, the angular resolution limit is $\Delta\theta^{th} = 1.22\lambda/D$, and the spatial resolution limit is $\Delta r^{th} = 1.22\Delta r_{out}$, Δr_{out} is the width of the outmost zone. Inserting the FZP parameters, one obtains $\Delta\theta^{th} = 2.4 \times 10^{-6}$ rad and $\Delta r^{th} = 0.43$ μm, in agreement with the numerical calculations. So the spatial resolution limit is not affected even for a total number of 100 zones.

FOV of the FZP

By placing a point source at different positions on the object plane, the FZP imaging is simulated and the FOV is obtained. For simplicity, a monochromatic point source is supposed and, for a typical case, the magnification is taken as $M = 10$, which means $p = 1.1f$, $q = 11f$. Figure 5 shows the image intensity distributions when the point source located at different positions in the object plane. For visibility, the intensity distributions of the off-axis images are displaced so that in all the cases the peak intensity is at position zero in the plot. When the point source is on the optical axis, the width from the intensity peak to the first minimum is 4.70 μm, the corresponding angular width $\Delta\theta = 2.4 \times 10^{-6}$ rad, in consistent with the minimum resolving angle of the FZP. In the present case, $p = 1.1f$, the spatial resolution is then $p \cdot \Delta\theta = 0.47$ μm, still very close to the spatial resolution limit, 0.43 μm, of the FZP.

Figure 5a also shows that when the point source is away from the optical axis to some extent, the image pattern starts to smear. In the intensity distribution, along with the decrease of the peak intensity, the wing becomes enhanced and the first minimum disappears. In this case, the image quality could be judged from the changing of the image's peak intensity. An acceptable tolerance for high-quality

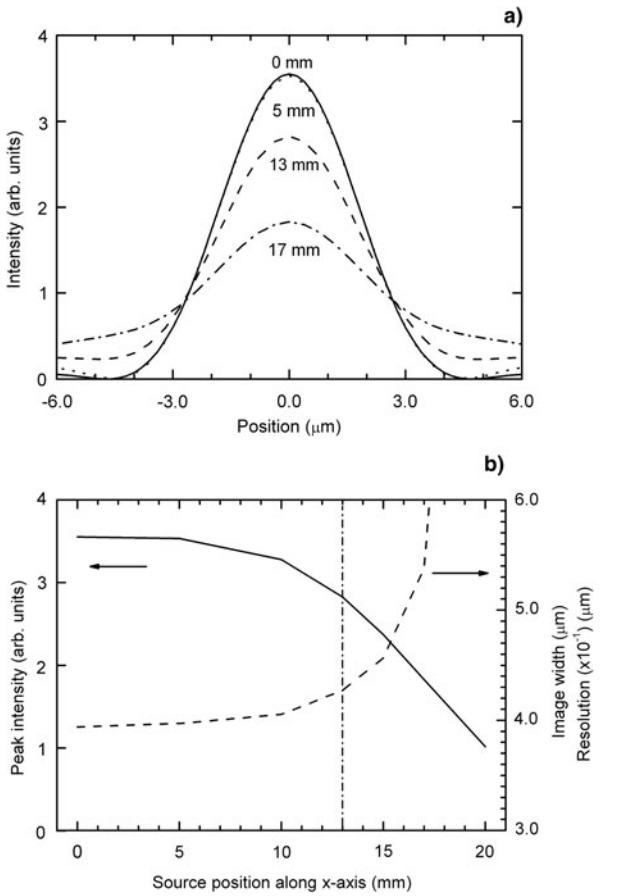

Fig. 5. (**a**) The intensity distribution of the FZP image when the point source is, along x-axis, at different positions from the optical axis. Solid line: the source on the optical axis. Dot line: the source is 5 mm away from the optical axis. Dash line: the source is 13 mm away. Dash-dot line: the source is 17 mm away. (**b**) The change of the image's peak intensity and width in FWHM with the point source position. Position 0 means the source is on the optical axis. The corresponding spatial resolution on the object plane is, defined by the Sparrow criterion, equal to the image width divided by the magnification. The dash-dot line denotes the source position where the image's peak intensity decreases by 20%.

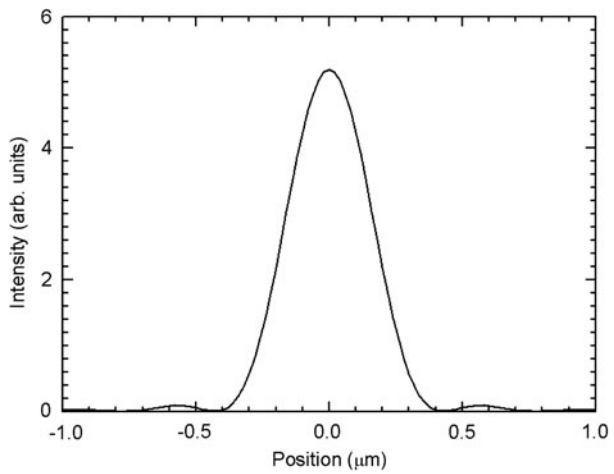

Fig. 4. The intensity distribution of the FZP focus along x-direction.

https://doi.org/10.1017/S0263034611000711 Published online by Cambridge University Press

imaging is, compared to the case when a point source is on the optical axis, the point source is away from the axis till its image's peak intensity decreases by 20% (Born & Wolf, 2001). The spatial resolution could be defined more conveniently by the so-called Sparrow criterion as the size in the object plane corresponding to the full width at half maximum (FWHM) of a point source's image. Note in the case of diffraction limit, the ratio of the Rayleigh resolution limit to the Sparrow resolution limit is 1.2.

As seen from Figures 5a and 5b, when the point source is off but close to the optical axis, e.g., 5 mm away, both the image's peak intensity and the FWHM almost do not change, which means that both the image quality and spatial resolution do not change as compared to the on-axis case. When the source is 13 mm away, the peak intensity decreases to 80% of that on the axis. But the image FWHM increases from 3.95 μm to 4.27 μm, less than 10% change. So, considering the symmetry of the FZP, an effective FOV for high-quality imaging is 26 mm (±13 mm away from the optical axis), corresponding to a viewing angle of 7.6°. Within it, the spatial resolution is close to the resolution limit and a high-quality image can be obtained as well. For a laser-fusion ignition target, its size is on the order of 10 mm, the FZP should be able to image, without changing the diagnostic setup, the whole or part of the target with a high resolution.

If the point source is further away from the optical axis, its image's peak intensity decreases quickly. For example, in Figure 5a, when the source is 17 mm away, the image's peak intensity decreases to 51% of that on the axis, and the wing is evidently enhanced. Obviously, the enhancement of the wing will lower the image contrast. Along with the decrease of the peak intensity, the spatial resolution also decreases evidently, as shown in Fig. 5(b). These two effects would deteriorate the image quality.

Influence of Polychromatic Light on the FZP Imaging

When the incident light is not monochromatic, for example, it is the mix of the *K*α line and continuum, or other *K*-shell lines, the influence of the spectral bandwidth on the FZP imaging has to be considered. Suppose the incident light is spectrally centered at $\lambda_0 = 0.275$ nm, with a bandwidth $\lambda_0 \pm \Delta\lambda/2$, in which the spectral density is constant. By varying the $\Delta\lambda/\lambda$ but keeping the same spectrally-integrated intensity, the FZP imaging of an on-axis point source is simulated using Eq. (7), the influence of polychromatic light can be found.

Figure 6 shows for $M = 10$ the change of image's peak intensity and FWHM versus the spectral bandwidth. When the bandwidth is increased to some extent, the peak intensity decreases, and the wing is enhanced that is similar to the phenomenon in Figure 5a, which would lower the image contrast. Compared to the monochromatic imaging, when the spectral bandwidth of a polychromatic light is increased to $\Delta\lambda/\lambda = 1.75\%$, the image's peak intensity decreases to 80%. However, the FWHM of the image changes from

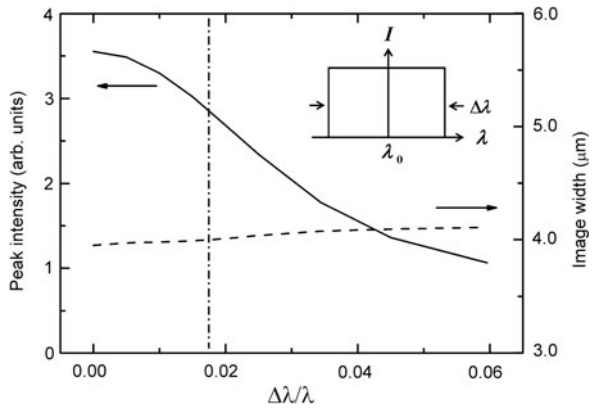

Fig. 6. The change of the image's peak intensity and width in FWHM with the spectral bandwidth. The dash-dot line denotes the spectral bandwidth, for which the image's peak intensity decreases by 20%. The inset shows the spectral intensity distribution for modeling a polychromatic incident light.

3.95 μm to 4 μm, only 1% variation, which means that the spatial resolution is almost unchanged. This indicates that the influence of the spectral bandwidth on the FZP imaging is mainly to lower the image contrast. Therefore, for the X-ray radiography application with the FZP as an imager, if the spectral bandwidth of the recorded image is controlled to be less than 1.75%, high-quality imaging could be realized.

The influence of the polychromatic light on the FZP imaging could be interpreted by the chromatic property of the FZP. In Eq. (8), the FZP's focal length is $f = r_1^2/\lambda$. Given the objective and the imaging distances, only the light of the wavelength λ_0 and those very close to the wavelength could be imaged well on the image plane at the imaging distance $q = q(\lambda_0)$, at which the images by the other wavelengths will be smeared. Numerical calculations reveal that for a monochromatic light of the same intensity as that of the λ_0, if its wavelength is 0.5% off the λ_0, the image's peak intensity will decrease to 80% of that of the λ_0. Therefore, for the FZP imaging of a polychromatic light, the contributions to the image are only from the wavelength λ_0 and the very nearby wavelengths. Thus, the chromatism of the FZP makes it capable of forming a monochromatic image at the λ_0.

DISCUSSIONS

The above results show that for X-ray imaging, the spatial resolution and the FOV of the FZP are much better than those of the K-B microscope. The resolution of the K-B microscope is limited by aberrations. For the FZP, working at normal incidence, the aberrations are avoided, and the spatial resolution is equal or close to the diffraction limit. Second, the spatial resolution of the K-B microscope decreases rapidly as its FOV increases to ± 200 μm. But for the FZP, the spatial resolution is close to the diffraction limit within a large FOV of 26 mm. So, such a K-B microscope is only appropriate for a high-resolution imaging of

https://doi.org/10.1017/S0263034611000711 Published online by Cambridge University Press

smaller FOV, but the FZP can be applied to a much wider FOV. It is anticipated that the FZP will be unique in X-ray imaging of a high resolution and a large FOV.

The efficiency of the two imagers can be compared. For a single spherical mirror of golden surface, at grazing incidence of θ_1 or θ_2, the reflectivity at 0.275 nm is about 50% (Henke *et al.*, 1993), then the total reflection for the K-B microscope is 25%. If the surfaces of the K-B mirrors are replaced by iridium, the total reflection will be 36%. For the FZP, the efficiency is calculated to be 18%. For the same collecting angle as given in Tables 1 and 2, the efficiency of the K-B microscope with *Ir* surfaces is about two times of that of the FZP. If the grazing-incidence angle θ_1 and θ_2 are decreased to 0.4°, the total reflection of the K-B microscope will be 64%, three times higher than that of the FZP. So a K-B microscope is more appropriate for imaging a not-so-bright source.

For the FZP imaging, the direct light, or the zeroth-order diffraction of the FZP, would form a primary background on the image plane and thus degrade the image quality. Several approaches have been adopted to improve the image quality, e.g., by inserting a central stop to block the zeroth order (Kirz, 1974; Michette, 1986). For the present FZP imaging, due to the phase shift caused by the FZP opaque zones, the efficiency of the first-order diffraction is increased to 18% of the incident light, and the background by the zeroth order is decreased to 9%. Thus, even not using a central stop, the image contrast is nearly 0.5, which should be enough to obtain information of the image. An advantage of the FZP imaging is to see tiny-spot structures such as filaments in an extended source. The sharp images of the tiny spots, though superimposed on the background, should be much easier to be discriminated. However, in imaging of an extended source, if the source is spatially coherent, the 0th-order light from the different positions of the source may interfere each other and cause spatial structures in the background, which would disturb the image. So a spatially incoherent extended source, which is common for laser plasmas and fusion targets and is supposed in the present analysis, should be able to avoid such interferences.

Finally, the influence of the polychromatic light on the two imagers is different. For the K-B microscope, there is no chromatic effect. By adding a reflection layer on the K-B mirror surfaces, a monochromatic image could be obtained (Mu *et al.*, 2009). For the FZP, the chromatism would decrease the image quality by lowering the contrast, so a monochromatic or a narrow spectral bandwidth is preferred. By selecting a line emission (Dasilva *et al.*, 1992), or combining with a multilayer mirror (Cauchon *et al.*, 1998), or adding absorption filters in the imaging setup (Azechi *et al.*, 2003), it should be possible to realize monochromatic imaging with the FZP.

CONCLUSIONS

The FZP imaging at the Ti *K*α line is analyzed in the regime where the Fresnel approximation cannot be applied. The proposed FZP has a spatial resolution limit of 0.43 μm. For such an FZP and a typical experimental setup with an image-to-object magnification of 10, a large FOV of 26 mm could be obtained, within which the FZP imaging has a spatial resolution close to the resolution limit. Compared to the imaging by a K-B microscope under similar experimental configurations, the K-B microscope has the best resolution of 0.71 μm at the FOV center and the resolution decreases significantly to 6 μm when the FOV is increased to about 400 μm. For polychromatic light illumination in the FZP imaging, if the spectral bandwidth is within 1.75%, a high-quality image can still be obtained. These results indicate the unique advantages of applying an FZP in high-resolution, large field-of-view X-ray imaging of laser-fusion targets, laser-plasma or other X-ray sources.

ACKNOWLEDGMENTS

This work was partially supported by the China National Hi-Tech Program and by the Chinese Academy of Sciences under Grant No. KJCX2-YW-N36.

REFERENCES

Azechi, H., Sakaiya, T., Fujioka, S., Tamari, Y., Otani, K., Shigemori, K., Nakai, M., Shiraga, H., Miyanaga, N. & Mima, K. (2007). Comprehensive diagnosis of growth rates of the ablative Rayleigh-Taylor instability. *Phys. Rev. Lett*. **98**, 045002.

Azechi, H., Tamari, Y. & Shiraga, H. (2003). Fresnel phase zone plates for Rayleigh-Taylor instability and implosion diagnostics. *Institute of Laser Engineering Annual Reports*. Osaka: Osaka University. 100–103.

Born, M. & Wolf, E. (2001). *Principles of Optics*. Cambridge: Cambridge University Press.

Cauchon, G., Pichet-Thomasset, M., Sauneuf, R., Dehz, P., Idir, M., Ollivier, M., Troussel, P., Boutin, J.-Y. & Lebreton, J.-P. (1998). Imaging of laser produced plasma at 1.43 keV using Fresnel zone plate and Bragg–Fresnel lens. *Rev. Sci. Instrum*. **69**, 3186–3193.

Chao, W., Harteneck, B.D., Liddle, J.A., Anderson, E.H. & Attwood, D.T. (2005). Soft X-ray microscopy at a spatial resolution better than 15 nm. *Nat*. **435**, 1210–1213.

Collins, G.W., Dasilva, L.B., Celliers, P., Gold, D.M., Foord, M.E., Wallace, R.J., Ng, A., Weber, S.V., Budil, K.S. & Cauble, R. (1998). Measurements of the equation of state of deuterium at the fluid insulator-metal transition. *Sci*. **281**, 1178–1181.

Dasilva, L.B., Trebes, J.E., Mrowka, S., Barbee, T.W., Brase, J., Koch, J.A., London, R.A., Macgowan, B.J., Matthews, D.L., Minyard, D., Stone, G., Yorkey, T., Anderson, E., Attwood, D.T. & Kern, D. (1992). Demonstration of x-ray microscopy with an x-ray laser operating near the carbon K edge. *Opt. Lett*. **17**, 754–756.

Gotchev, O.V., Jaanimagi, P.A., Knauer, J.P., Marshall, F.J., Meyhofer, D.D., Bassett, N.L. & Oliver, J.B. (2003). High-throughput, high-resolution Kirkpatrick–Baez microscope for advanced streaked imaging of ICF experiments on OMEGA. *Rev. Sci. Instrum*. **74**, 2178–2181.

Henke, B.L., Gullikson, E.M. & Davis, J.C. (1993). X-ray interactions: photoabsorption, scattering, transmission, and reflection at E = 50–30000 eV, Z = 1–92. *At. Data Nucl. Data Tables* **54**, 181–342.

Kirkpatrick, P. & Baez, A.V. (1948). Formation of optical images by X-rays. *J. Opt. Soc. Am.* **38**, 766–774.

Kirz, J. (1974). Phase zone plates for X-rays and the extreme UV. *J. Opt. Soc. Am.* **64**, 301–309.

Koch, J.A., Aglitskiy, Y., Brown, C., Cowan, T., Freeman, R., Hatchett, S., Holland, G., Key, M., Mackinnon, A., Seely, J., Snavely, R. & Stephens, R. (2003). 4.5- and 8-keV emission and absorption x-ray imaging using spherically bent quartz 203 and 211 crystals. *Rev. Sci. Instrum.* **74**, 2130–2135.

Lindl, J.D., Amendt, P., Berger, R.L., Glendinning, S.G., Glenzer, S.H., Haan, S.W., Kauffman, R.L., Landen, O.L. & Sute, L.J. (2004). The physics basis for ignition using indirect-drive targets on the National Ignition Facility. *Phys. Plasmas* **11**, 339–491.

Liu, L.H., Liu, G., Ying, X., Chen, J., Kang, C.-L., Huang, X.-L. & Tian, Y.-C. (2008). Fabrication of Fresnel zone plates with high aspect ratio by soft X-ray lithography. *Microsyst. Technol.* **14**, 1251–1255.

Marshall, F.J., Allen, M.M., Knauer, J.P., Oertel, J.A. & Archuleta, T. (1998). A high-resolution x-ray microscope for laser-driven planar-foil experiments. *Phys. Plasmas* **5**, 1118–1124.

Marshall, F.J. & Bennett, G.R. (1999). A high-energy x-ray microscope for inertial confinement fusion. *Rev. Sci. Instrum.* **70**, 617–619.

Michette, A.G. (1986). *Optical Systems for Soft X-rays*. New York: Plenum Press.

Mu, B.-Z., Wang, Z.-S., Yi, S.-Z., Wang, X., Huang, S.-L., Zhu, J.-T. & Huang, C.-C. (2009). Study of X-ray Kirkpatrick-Baez imaging with single layer. *Chin. Opt. Lett.* **7**, 452–454.

Stigliani, D.J., Mittra, R. & Semonin, R.G. (1967). Resolving power of a zone plate. *J. Opt. Soc. Am.* **57**, 610–613.

Taguchi, T., Antonsen, T.M., Liu, C.S. & Mima, K. (2001). Structure formation and tearing of an MeV cylindrical electron beam in a laser-produced plasma. *Phys. Rev. Lett.* **86**, 5055–5058.

Tian, Y.C., Li, W., Chen, J., Liu, L., Liu, G., Tkachuk, A., Tian, J., Xiong, Y., Gelb, J., Hsu, G. & Yun, W. (2008). High resolution hard x-ray microscope on a second generation synchrotron source. *Rev. Sci. Instrum.* **79**, 103708.

Wang, J.-Y., Chen, X.-G. & Wang, X.-F. (2010). Kirkpatrick-Baez mirror imaging simulation and comparison with Fresnel zone plate imaging. *Acta Photon. Sin.* **39**, 2158–2162.

Wang, X.-F. & Wang, J.-Y. (2011). Analysis of high-resolution X-ray imaging of an inertial-confinement-fusion target by using a Fresnel zone plate. *Acta Phys. Sin.* **60**, 025212.

https://doi.org/10.1017/S0263034611000711 Published online by Cambridge University Press